Available online at www.sciencedirect.com
ScienceDirect
Journal of the European Ceramic Society 28 (2008) 2019–2024
www.elsevier.com/locate/jeurceramsoc

Dilatometer analysis of sintering behavior of nano-CeO_2 particles

Yoshiaki Kinemuchi *, Koji Watari

National Institute of Advanced Industrial Science and Technology (AIST), 2266-98 Anagahora, Shimoshidami, Moriyama, Nagoya 463-8560, Japan

Received 21 June 2007; received in revised form 22 January 2008; accepted 1 February 2008
Available online 18 April 2008

Abstract

Dilatometer analysis was conducted for nano-CeO_2 particles, with varying green densities. Bimodal shrinkage rate was noticed for nano-particles with respect to temperature, while single mode was observed for submicron particles. With decrease in green density, the intensity of the low temperature peak in the bimodal shrinkage rate increased compared with that of high temperature peak. The activation energies of nano-CeO_2 sintering estimated by the master sintering curve were 370 and 440 kJ/mol for temperature ranges near the low temperature peak and near the high temperature peak, respectively, while the activation energy of submicron-CeO_2 sintering was 420 kJ/mol. It was found that the low temperature peak characterized the sintering behavior of nano-CeO_2, and this peak was responsible for the enhancement in the sinterability of green compact with low density.

Keywords: Sintering; Surfaces; CeO_2

1. Introduction

Nano-particles have the advantage of low temperature process owing to their high surface energy, although there are difficulties in the forming process due to strong agglomeration of particles. Hence it is believed that the primary method to achieve reliable processing depends on the dispersion process. The sintering process is steadily influenced by the state of green bodies, and low green density results in high sintering temperature. This originates from the fact that large pores commonly existing in green bodies with low density require high sintering temperature to be eliminated. In general, strong agglomeration of nano-particles is considered a primary hindrance to achieve low temperature process, because these aggregates tend to form large pores at their neighbors during sintering.

On the contrary, Chen and Chen[1] found that the nano-particles of CeO_2 prepared by homogeneous precipitation method possessed superior sintering ability that enabled them to densify at much lower temperatures than that of submicron particles. Interestingly, the densification temperature was independent of the green density,[2] indicating faster shrinkage rate of specimens with lower green density. They concluded that this intrinsic behavior originated in the particle rearrangement due to the enormous grain growth of nano-particles.

Another interesting shrinkage phenomenon of nano-CeO_2 particles was reported by Ozawa.[3] He observed the sintering progress by dilatometric method and found bimodal shrinkage behavior. The first peak of bimodal shrinkage appeared at 730 °C and the second peak appeared at 1300 °C. At the first peak there was a simultaneous weight loss, which may correspond to $CeO_2 = CeO_{2-x} + (x/2)O_2$. Based upon the observed behavior, they considered bimodal shrinkage was owing to the reduction of nano-CeO_2 particles.

The redox reaction of nano-CeO_2 particles is widely used in industry, which is applied to an automotive exhaust catalyst as oxygen storage. In this application, chemisorption of oxygen is effectively utilized to promote oxidation activity and to widen air–fuel ratio window where major pollutants such as HC, CO and NO can be removed.[4] In addition, the enthalpy of reduction of nano-CeO_2 was reported to be 1.84 eV (177 kJ/mol),[5] which was less than half of that of bulk CeO_2 of 4.67 eV (450 kJ/mol).[6,7]

Previous reports concerning the transport of CeO_2 indicate that the non-stoichiometry of CeO_2 plays an important role, which comes from the ionic nature of CeO_2. Then we can assume that the sintering rate of CeO_2 is primarily governed by the formation of oxygen vacancy. In order to confirm this assumption, we analyze the activation energy of sintering by

* Corresponding author. Tel.: +81 52 736 7697; fax: +81 52 736 7697.
E-mail address: y.kinemuchi@aist.go.jp (Y. Kinemuchi).

0955-2219/$ – see front matter © 2008 Elsevier Ltd. All rights reserved.
doi:10.1016/j.jeurceramsoc.2008.02.003

the master sintering curve[8] and discuss the sintering behavior of nano-CeO_2.

2. Experimental procedures

Commercially available CeO_2 particles (NanoTek, Kanto Kagaku, Japan) were utilized as starting particles. These particles are synthesized by physical vapor synthesis and have rectangular morphology (see Fig. 1a). The purity of the particles is 99.8% and BET specific surface area was 65.1 m^2/g. In order to distinguish the nano-particle effect, submicron particles were also utilized. Submicron particles were prepared from commercially available particles (Junsei Kagaku, Japan). Since the commercial particles were granulated and consisted of nano-particles, we heat-treated them at 1200 °C for 1 h. Subsequently, the particles were planetary-milled by using Al_2O_3 balls for 2 h at 300 rpm, and the particles were used for the experiment as submicron particles. The BET specific surface area of the submicron powder was found to be 5.13 m^2/g, and the averaged particle size was 0.6 μm measured by LASER scattering particle size distribution analyzer. Particle morphology of submicron particles is shown in Fig. 1b. X-ray diffraction patterns of these particles were confirmed as cubic structure without minor phase. The particles were pelletized into rectangular bars by dry pressing. Here no lubricant or binder was used. Pressing was carried out by uni-axial pressing and subsequently by cold isostatic pressing (CIP), and the CIP pressure was varied from 5 to 150 MPa in order to control the green density. The typical size of green bodies was 10 mm × 5 mm × 5 mm, and the size, becomes larger with lower CIP pressure.

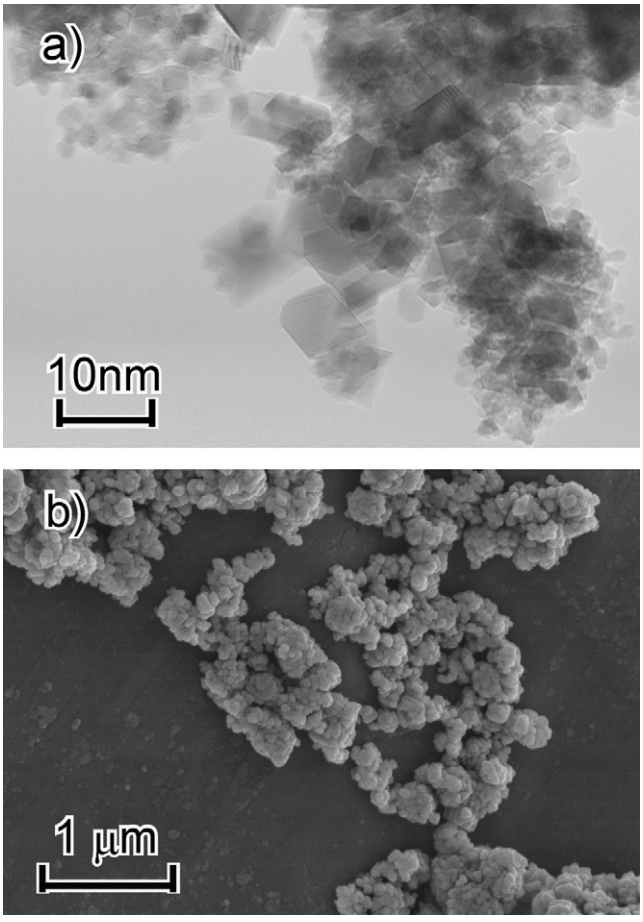

Fig. 1. Morphology of particles: (a) nano-particles and (b) submicron particles.

Sintering behavior was monitored by a differential dilatometer (TD5200SA, Bruker-Japan, Japan) measuring linear deformation of the rectangular bars lengthwise. The accuracy of the dilatometer is 0.1 μm. During the monitoring, a load of 10 g was applied in order to ensure the physical contact between specimens and specimen holders. For the referenced material during the measurement, polycrystalline Al_2O_3 column was used. Then the monitored displacement was corrected based on the thermal expansion of the referenced Al_2O_3. The transient length of the specimens was obtained by the summation of the monitored displacement and the initial length of the specimen. Heating was carried out from room temperature to 1500 or 1600 °C at the heating rate of 1, 5, 10 or 15 °C/min. The maximum temperature was held for 1 min. Subsequent cooling was carried out at the rate of 10 °C/min. Flow of air was maintained at the rate of 50 ml/min during measurement. Displacement was found to shift toward the direction of shrinkage during heating and the direction of expansion during cooling. The former deformation was mainly caused by sintering of the specimen and the latter originated in thermal expansion of the specimen. Thus monitored length of specimen during heating included the thermal expansion, and density shown in this paper is transient density calculated on the monitored length. Above shrinkage monitoring was carried out twice for each condition, and good reproducibility was confirmed.

Based on the displacement during both heating and cooling, density of the specimen was evaluated assuming isotropic shrinkage:

$$\rho_t = \rho_0 \exp(-3\varepsilon_t) \tag{1}$$

Here, ρ_t is transient density and ρ_0 is density at the reference condition and ε_t is true strain that is defined by the following equation:

$$\varepsilon_t = \ln\frac{l_t}{l_0} \tag{2}$$

Here, l_t is the transient length of the sample and l_0 is the length of the reference condition. For the reference condition, we selected the specimen after cooling, since the accurate density was available compared with green density. As seen in Eq. (1), weight change of sample during measurement was not considered in the transient density.

Density of green body was measured from the weight of the specimen and its dimension, and sintered density that was used as reference value in Eq. (1) was measured by Archimedean method.

Activation energy of sintering was evaluated based on the master sintering curve (MSC).[8] Here, the measured transient density was plotted to the function $\Theta(t, T(t))$ which is defined as

$$\Theta(t, T(t)) \equiv \int_0^t \frac{1}{T} \exp\left(-\frac{Q}{RT}\right) \mathrm{d}t \tag{3}$$

where t is time, T the absolute temperature, Q the apparent activation energy of sintering, and R the gas constant. The series of the transient densities measured at different heating rates were plotted versus $\Theta(t, T(t))$ using an activation energy. Then the least square method was adopted to converge all the lines on the one line, so-called master sintering curve, by tuning the activation energy. The optimized activation energy was denoted as the activation energy of sintering. It is reported that the activation energy derived by MSC reasonably agrees with that obtained by other method.[8] The accuracy of optimized activation energy was found to be ± 10 kJ in the present experiment. As shown in Eq. (3), MSC assumes single activation energy although sintering involves different diffusion paths such as surface diffusion, grain boundary diffusion and volume diffusion. Thus obtained activation energy by MSC reflects the most governing mechanism during densification. Because of this assumption, MSC sometimes shows deviation from measured curves at low or high densities due to surface diffusion or exaggerated grain growth.[8] In other words, it is possible to detect the influence of other sintering mechanisms by observing deviation from MSC. Since procedure to obtain MSC is statistical fitting method, we can adopt it to a local density region. Consequently several activation energy will be obtained at the local region, which can be considered as the activation energy of dominant sintering mechanism at the density region. We adopted this procedure when the deviation was found in the curve fitting.

3. Results and discussion

Fig. 2 indicates a densification process of both nano-particles and submicron particles with differing green density. Here several peculiarities are noticed in the sintering of nano-particles. First, there is no clear on-set temperature of shrinkage. Second, shrinkage is terminated at ca. 1300 °C, while submicron particles continued to shrink up to 1600 °C, which was the maximum temperature of our heater. Third, the shrinkage rate was greatly influenced by green density. That is, samples with low green density showed faster shrinkage, and the density curves of different green densities converged at 1300 °C. In contrast to nano-particles, submicron particles showed a shift of the shrinkage curve toward higher temperatures with decrease in green density. Fourth, final density increased by lowering green den-

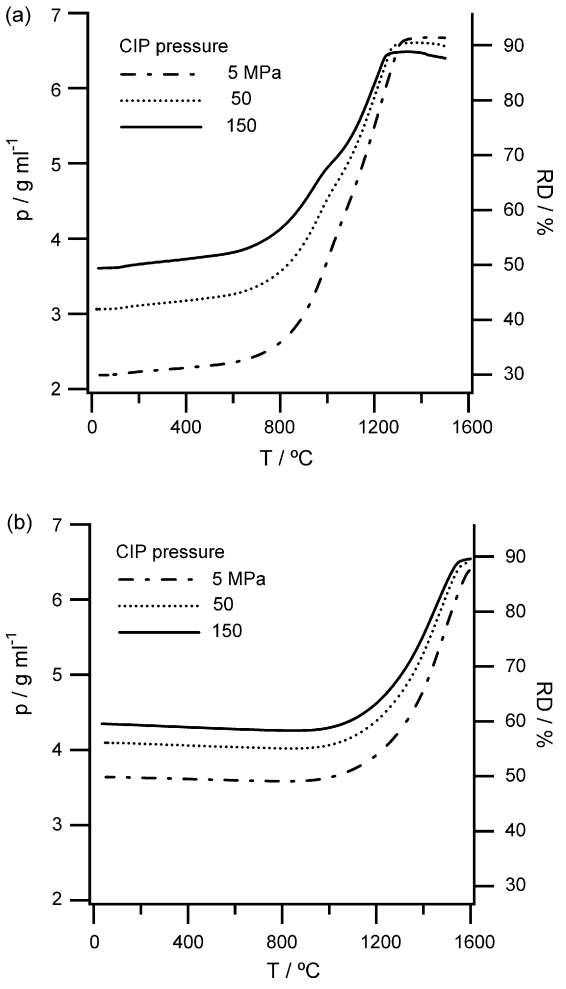

Fig. 2. Densification curves of samples with various green densities as a function of temperature: (a) nano-particles and (b) submicron particles.

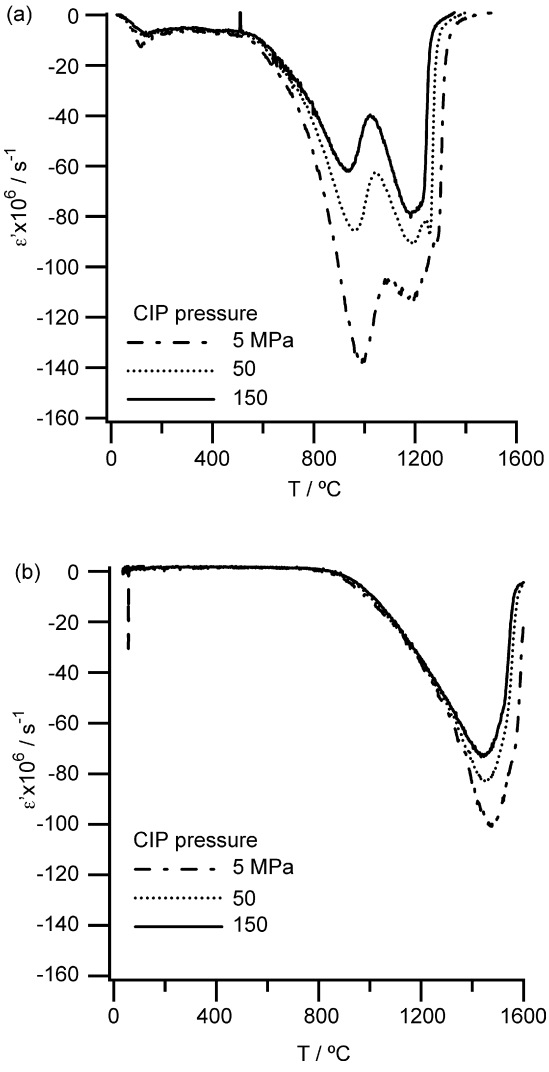

Fig. 3. Shrinkage rates of samples with various green densities as a function of temperature: (a) nano-particles and (b) submicron particles.

sity, while submicron particles showed similar density without much influence of green density. Among the several peculiar features of nano-particles, the influence of green density on their sintering behavior is quite interesting in terms of particle processing, as mentioned in Section 1. Regarding the influence of green density on the shrinkage behavior, Chen and Chen reported a similar tendency for nano-CeO_2 particles prepared by precipitation method.[1] In their report, dry pressed pellets showed different green densities due to various calcination temperatures. Variance of green density in their report ranged from 2.9 to 3.7 g/ml. Although this difference in green density may originate in state of aggregation during calcination, the shrinkage curve was converged on one point as in the present observation. They pointed out that nano-particles with inherently better sinterability possess a larger tolerance for the handling and green compaction methods. Later, they proposed coarsening-motivated homogenization and rearrangement densification processes, which account for the remarkable sinterability, even at a very low density.[2] Since this model is based on particle rearrangement due to grain growth, there is an upper limit of the applicable region of sintering progress. Above the relative density of 0.65, particles become closely packed, thus the rearrangement may hardly occur.[2]

Fig. 3 shows the linear shrinkage rate as a function of temperature, showing large influence of green density on the shrinkage rate. Here, nano-particles with a lower green density kept the higher shrinkage rate through the entire heating process. This behavior also can be seen in submicron particles. It is also noted that nano-particles showed bimodal shrinkage behavior that was already reported by Ozawa[3] and Zhou and Rahaman.[9] Both groups pointed out the importance of redox reaction of CeO_2 on its sintering behavior. Zhou et al. concluded that the CeO_2 released the oxygen above 1200 °C, which resulted in a decrease in density due to microcracking. They also pointed out that released oxygen produced additional pores, requiring high sintering temperature. Ozawa reported that the oxygen release around 700 °C enhanced the sintering rate and the shrinkage peak at this temperature was only observed in nano-CeO_2. In the catalysis application of CeO_2, it is well known that nano-CeO_2 shows two peaks of oxygen release with respect to temperature, and the peaks correspond to the reduction at the surface and in the bulk of CeO_2, respectively.[4] In addition, the reduction at the

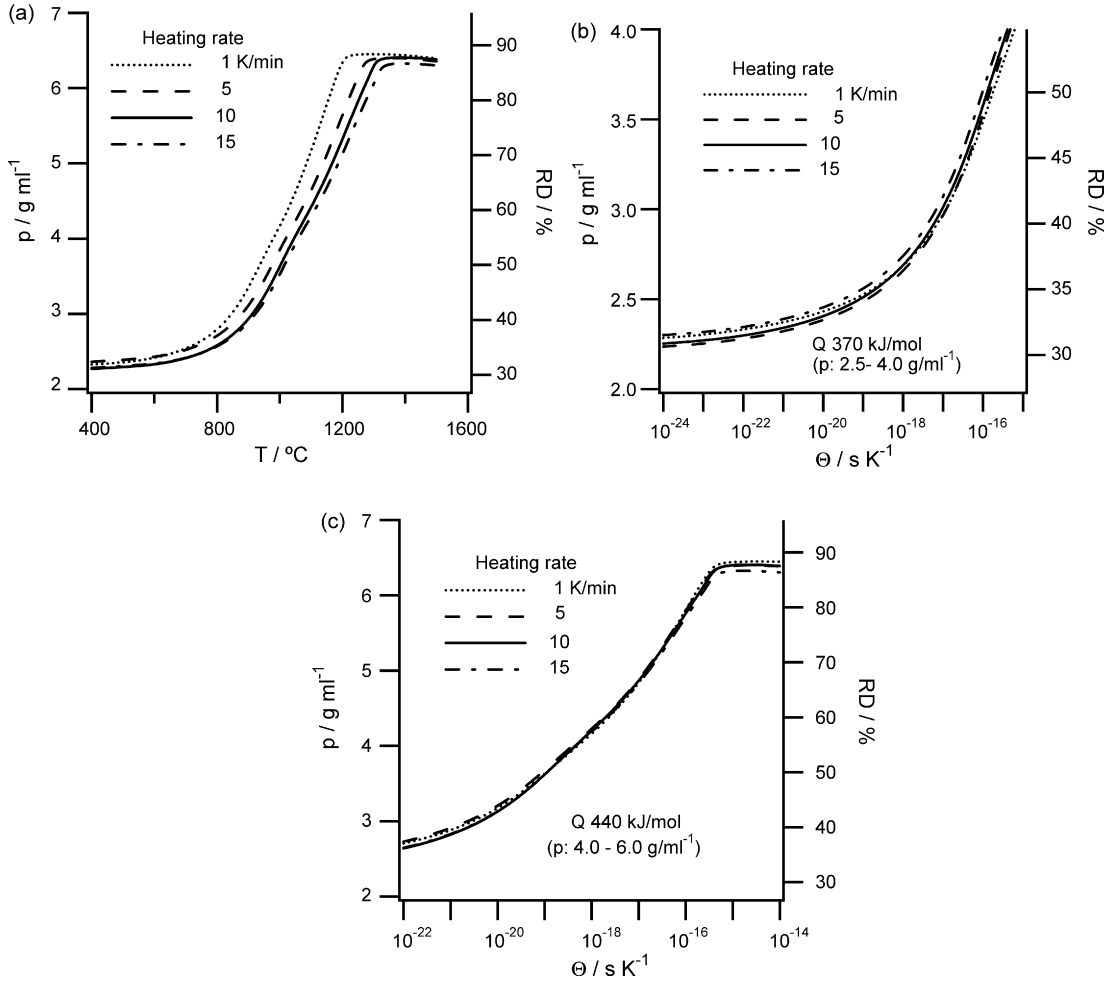

Fig. 4. Original densification curves (a) and master sintering curve of nano-CeO_2 particles at the temperature regions where the low temperature peak of shrinkage rate was observed (b) and where the high temperature peak of shrinkage rate was observed (c).

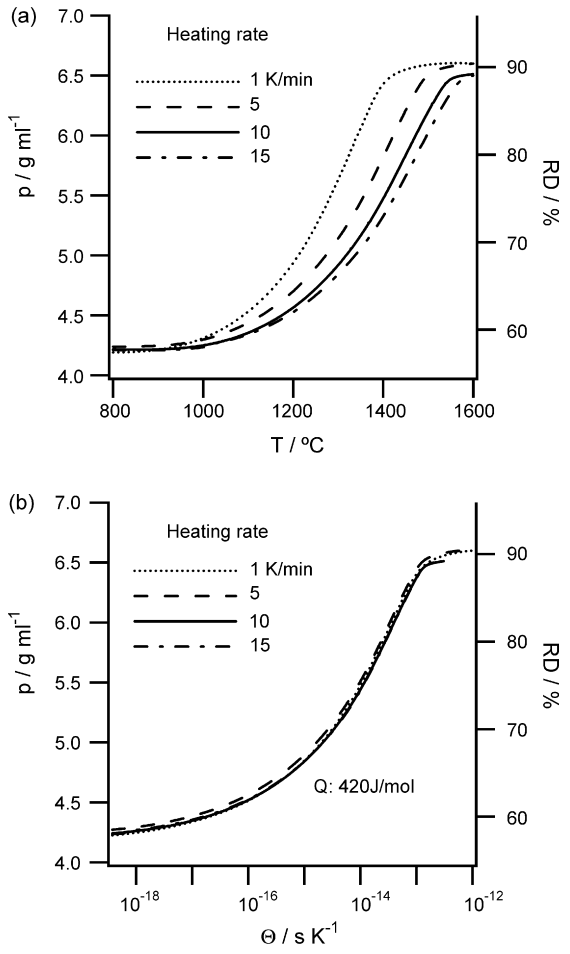

Fig. 5. Original densification curves (a) and master sintering curve (b) of submicron-CeO_2 particles.

low temperature does not occur in submicron particles.[10] Therefore, the peak of shrinkage rate at low temperature is thought to be correlated with oxygen release at the surface. It is probable that oxygen vacancies near surface enhance grain boundary diffusion, leading to an increase in the shrinkage rate.

In contrast to nano-particles, the submicron particles showed shrinkage rate of single mode, and the peak appeared at relatively high temperature, suggesting a large contribution of volume diffusion to the shrinkage.

It is noted that the shape of the shrinkage rate is also influenced by green density in case of nano-CeO_2. The bimodal shape was maintained, regardless of the difference in green density. However, the peak intensity of each peak gradually changed with green density, where the low temperature peak became dominant for the low green density. This means that the shrinkage enhancement in low green density originates in the low temperature peak.

Since there was significant difference in sintering behaviors between submicron and nano-particles, the activation energy of sintering was estimated by MSC (Figs. 4 and 5). For the submicron particles, the activation energy was estimated to be 420 kJ/mol, which corresponded to the enthalpy of the reduction of bulk CeO_2. This suggests that the diffusion of CeO_2 is governed by the formation of oxygen vacancy, and thus sintering rate is determined by oxygen diffusion. For the nano-particles, MSC was adopted at the two regions, namely near the low temperature peak or the high temperature peak of the shrinkage rate. The obtained activation energies were 370 and 440 kJ/mol at the low temperature peak and the high temperature peak, respectively. The activation energy of high temperature peak was almost identical with that of submicron particles. The relatively low activation energy found at the low temperature peak is plausible, if the surface reduction of nano-CeO_2 is contributed to the diffusion. Besides, it can be also understood that the difference in the activation energies is the reflection of the difference in sintering mechanism, that is the sintering is dominated by grain boundary diffusion or volume diffusion. Because the grain boundary diffusion is considered to be remarkable at the initial sintering stage, the activation energy of initial sintering in submicron particles was also estimated by MSC, where applied density range was from 4.5 to 5.0 g/ml (relative density (RD) of 0.6–0.7). Interestingly, the obtained activation energy was 430 kJ/mol, which implies that this activation energy is intrinsic to the sintering of submicron particles. Thus, it was also clarified that the low temperature peak with low activation energy is a unique sintering behavior of nano-CeO_2.

In order to further clarify the influence of green density on the shrinkage rate, the latter is plotted as a function of density (Fig. 6). This analysis was carried out by Rahaman et al.[11] in ZnO, showing a clear influence of green density on shrinkage. In their experiment, lower green density maintained higher shrinkage rate up to relative density of 0.8, and above the density, shrinkage rates of all samples almost coincided, in spite of different green densities. Similar tendency was found in the shrinkage of submicron particles. A higher shrinkage rate was observed for samples with a lower green density up to 6.0 g/ml that is RD of 0.82, and above this density, shrinkage rate was independent of the green density. In other words, the shrinkage rate at the final sintering stage can be expressed only by the function of density. As regards nano-particles, the shrinkage was maintained at a higher rate in lower green density, similar to the submicron particles, and this tendency was maintained even at high density. As mentioned earlier, Chen and Chen[2] proposed the coarsening-motivated homogenization and rearrangement densification mechanism, and they concluded that the mechanism explained the influence of green density on the shrinkage. As their analysis indicates, the applicable region of this mechanism seems to be until initial sintering stage (RD < 0.6). However, high sinterability of green compact with low green density was observed up to the density of 6.5 g/ml (RD < 0.9) in the present study, which is apparently beyond the region of their model.

So far, there was no probable model to explain the behavior of nano-CeO_2 particles. However, as seen in the emergence of the low temperature peak in the shrinkage rate of nano-CeO_2, the reduction of the surface during heating is thought to be responsible for the peculiar character of nano-CeO_2 sintering. This surface reduction may lead to an enhancement in grain boundary diffusion, which greatly influences the sintering behavior, even at the final stage of sintering.

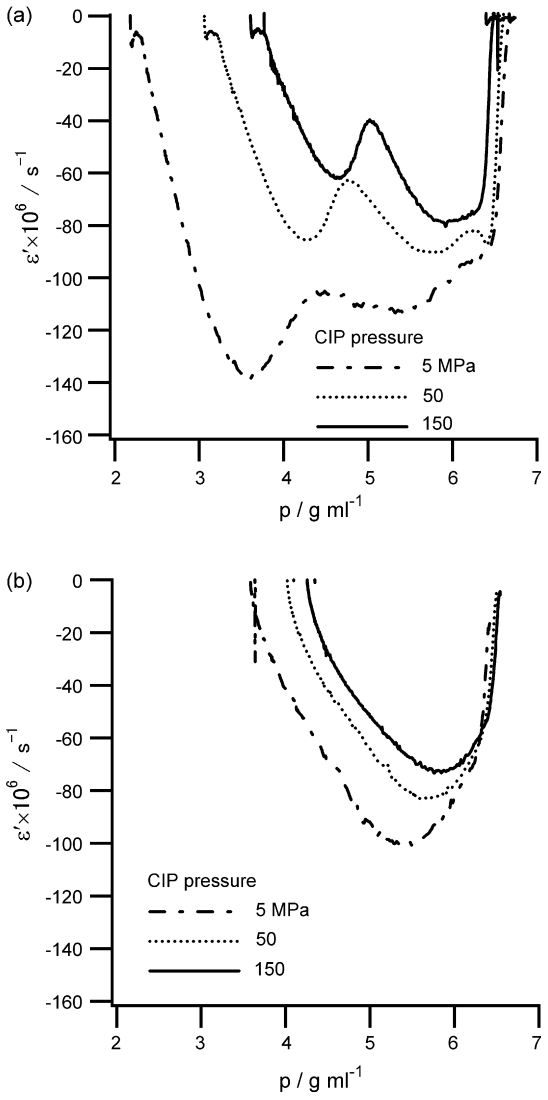

Fig. 6. Shrinkage rates of samples with various green densities as a function of density: (a) nano-CeO_2 and (b) submicron-CeO_2 particles.

4. Conclusions

Sintering behavior of commercially available nano-CeO_2 particles was monitored by dilatometer, with a focus on the influence of green density. With a comparison of shrinkage behavior of submicron particles, several unique behavioral traits of nano-CeO_2 shrinkage were observed as follows:

(1) Bimodal shrinkage rate was observed for nano-particles, while single mode was monitored for submicron particles. Here, low temperature peak of shrinkage rate was characteristic of nano-particles. The peak intensity of the low temperature peak increased with a decrease in green density, and the intensity ratio of the low temperature peak to high temperature peak also increased with a decrease in green density.

(2) The master sintering curve method was applied to estimate the activation energy of sintering. The obtained activation energies of nano-CeO_2 sintering were 370 and 440 kJ/mol at the low temperature peak and the high temperature peak, respectively. Besides, the activation energy of submicron-CeO_2 was estimated to be 420 kJ/mol, which corresponded to the enthalpy of the reduction of CeO_2.

(3) Shrinkage rate of low green density exceeded that of high green density through entire density region for nano-particles. Similar tendency can be seen in submicron particles up to the relative density of 0.8, however, above the density the shrinkage rate was independent of green density.

(4) Density curves of samples converged at 1300 °C, even though the green density varied from 2.2 to 3.6 g/ml (from RD of 0.31–0.51) for nano-CeO_2. Besides, submicron particles showed a shift of densification curve toward higher temperature with a decrease in green density.

These conclusions support the view that the low temperature peak at shrinkage rate is the fundamental behavior of nano-CeO_2, which effectively enhances the sintering of green compact with low packing density. The low temperature peak is caused by the surface reduction of nano-CeO_2.[3,4] Thus the surface chemistry plays an important role in the sintering of nano-CeO_2 particles.

References

1. Chen, P. L. and Chen, I. W., Reactive cerium(IV) oxide particles by the homogeneous precipitation method. *J. Am. Ceram. Soc.*, 1993, **76**(6), 1577–1583.
2. Chen, P. L. and Chen, I. W., Sintering of fine oxide particles. II. Sintering mechanisms. *J. Am. Ceram. Soc.*, 1997, **80**(3), 637–645.
3. Ozawa, M., Effect of oxygen release on the sintering of fine CeO_2 particle at low temperature. *Scripta Mater.*, 2004, **50**, 61–64.
4. Yao, H. C. and Yu Yao, Y. F., Ceria in automotive exhaust catalysts. I. Oxygen storage. *J. Catal.*, 1984, **86**, 254–265.
5. Hwang, J. H. and Mason, T. O., Defect chemistry and transport properties of nanocrystalline cerium oxide. *Z. Phys. Chem.*, 1998, **207**, S21–S38.
6. Kamiya, M., Shimada, E., Ikuma, Y., Komatsu, M. and Haneda, H., Intrinsic and extrinsic oxygen diffusion and surface exchange reaction in cerium oxide. *J. Electrochem. Soc.*, 2000, **147**(3), 1222–1227.
7. Tuller, H. L. and Nowick, A. S., Defect structure and electric properties of non-stoichiometric CeO_2 single crystal. *J. Electrochem. Soc.*, 1979, **126**(2), 209–217.
8. Su, H. and Johnson, D. L., Master sintering curve: a practical approach to sintering. *J. Am. Ceram. Soc.*, 1996, **79**(12), 3211–3217.
9. Zhou, Y. C. and Rahaman, M. N., Hydrothermal synthesis and sintering of ultrafine CeO_2 particles. *J. Mater. Res.*, 1993, **8**(7), 1680–1686.
10. Ozawa, M., Matsuda, K. and Suzuki, S., Microstructure and oxygen release properties of catalytic alumina-supported CeO_2–ZrO_2 powders. *J. Alloys Compd.*, 2000, **303–304**, 56–59.
11. Rahaman, M. N., De Jonghe, L. C. and Chu, M. Y., Effect of green density on densification and creep during sintering. *J. Am. Ceram. Soc.*, 1991, **74**(3), 514–519.